Journal of Alloys and Compounds, 200 (1993) 51–57
JALCOM 754

Magnetic structure of YMn_6Ge_6 and room temperature magnetic structure of $LuMn_6Sn_6$ obtained from neutron diffraction study

G. Venturini, R. Welter and B. Malaman
Laboratoire de Chimie du Solide Minéral, Université de Nancy I, associé au CNRS, UA 158, BP 239, 54506 Vandoeuvre les Nancy Cedex (France)

E. Ressouche
Centre d'Etudes Nucléaires de Grenoble, DRFMC/SPSMS, 85 X, 38041 Grenoble Cedex (France)

(Received March 10, 1993)

Abstract

Neutron diffraction measurements have been performed on the ternary compounds YMn_6Ge_6 and $LuMn_6Sn_6$ of $HfFe_6Ge_6$-type structure (space group, *P6/mmm*). This structure can be described as a filled derivative of the CoSn-B35-type structure. Each of the rare earth (R) and Mn atoms are successively distributed in alternate layers, stacked along the *c* axis with the sequence Mn–R–Mn–Mn–R–Mn. At 300 K, both compounds exhibit collinear antiferromagnetic arrangements and the magnetic structures consist of a stacking of ferromagnetic (001) layers of Mn with the coupling sequence Mn(+)–R–Mn(−)–Mn(−)–R–Mn(+) ($\mu_{Mn} \approx 1.33(1)\mu_B$ and $1.82(3)\mu_B$ for $LuMn_6Sn_6$ and YMn_6Ge_6 respectively). For $LuMn_6Sn_6$, the magnetic moments lie in the (001) plane, while they are along the *c* axis in YMn_6Ge_6. At low temperature, a spin reorientation process occurs in both compounds, yielding incommensurate antiferromagnetic arrangements. For YMn_6Ge_6 ($T_t \approx 80$ K), the Mn moments form a double-cone structure with a periodicity of about 105 Å ($\mu_{Mn} = 1.95(4)\mu_B$ at 2 K), while only preliminary results are available for $LuMn_6Sn_6$ below about 200 K. The results are compared with those obtained on the CoSn-B35-type structure binary compounds FeSn and FeGe, on one hand, and the RMn_6Sn_6 compounds, on the other hand.

1. Introduction

In previous papers we have reported on the crystallographic data of new ternary stannides RMn_6Sn_6 (R ≡ Sc, Y, Gd–Tm, Lu) [1, 2] and germanides RMn_6Ge_6 (R ≡ Sc, Y, Nd, Sm, Gd–Lu) [3]. All these compounds crystallize in the $HfFe_6Ge_6$-type structure (space group, *P6/mmm*) [4]. The crystal structure of $HfFe_6Ge_6$ is an ordered filled derivative of the CoSn-B35 type (space group, *P6/mmm*) adopted by the binary FeGe and FeSn compounds (Fig. 1) [5]. This structure can also be described as being built of alternate (001) layers containing R and transition metal (T) atoms respectively. R elements build hexagonal planes (H) and T elements build Kagomé nets (K), stacking along the *c* axis with the sequence ...KHKKHK... [6] (Fig. 1). As regards the transition metal and rare earth coordination polyhedra around the rare earth (Fig. 1), this structure is also closely related to the well-known $CaCu_5$- and $ThMn_{12}$-type structures [5]. From this point of view, it was rather interesting to study their magnetic properties.

Magnetization measurements on RMn_6Sn_6 (R ≡ Sc, Y, Gd–Tm, Lu) [6] and the germanides RMn_6Ge_6 (R ≡ Sc, Y, Nd, Sm, Gd–Lu) [3] as polycrystalline samples have been largely described. All the compounds with paramagnetic rare earths order ferro(antiferro)-magnetically up to rather high temperatures (333 K $< T_{C,N} <$ 516 K). Furthermore, in most cases, both the R and Mn sublattices order simultaneously above the room temperature. However, neutron diffraction studies on RMn_6Sn_6 (R ≡ Tb–Dy, Er at low temperature) compounds [7, 8] show that, in all cases, the magnetic structures consist of ferromagnetic (001) layers of R and Mn atoms stacked along the *c* axis with the coupling sequence Mn(−)–R(+)–Mn(−)Mn(−)–R(+)–Mn(−), yielding a ferrimagnetic behaviour. The thermal variations of the easy axis directions are given in Table 1. It appears that the magnetic easy direction shows a strong and somewhat systematic dependence on the identity of the rare earth element. It should be noted that complex, flat spiral structures are observed in $ErMn_6Sn_6$ above 50 K and in $TmMn_6Sn_6$ [8].

All the RMn_6X_6 compounds with diamagnetic R elements (Sc, Lu, Y) are characterized by an antifer-

0925-8388/93/$6.00

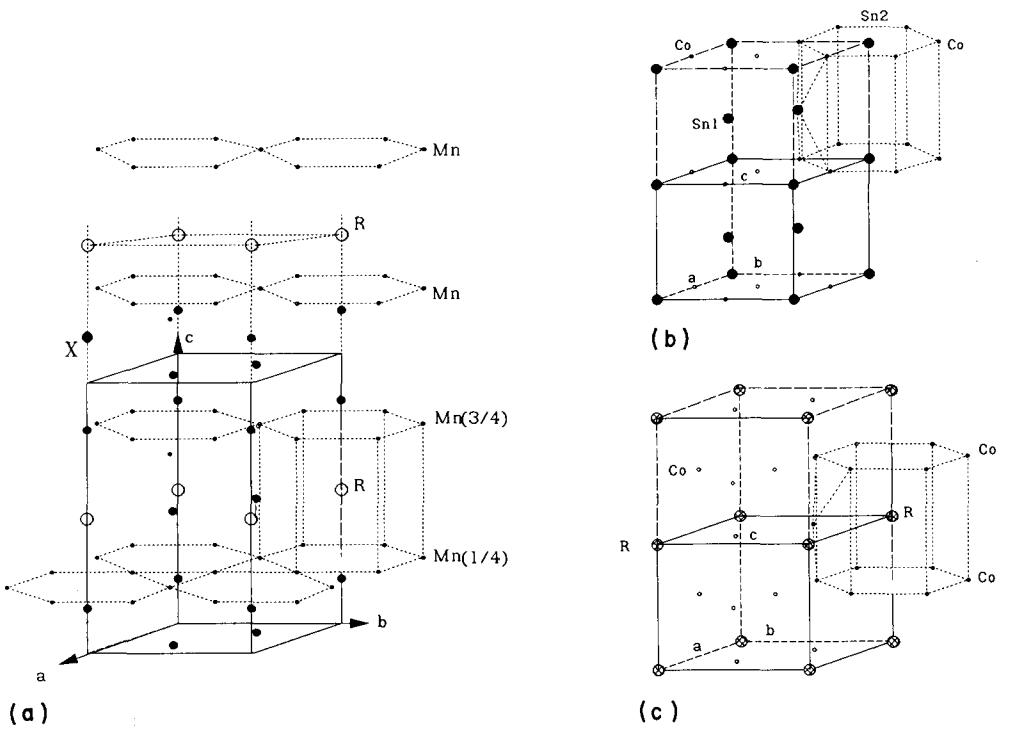

Fig. 1. Structures of (a) RMn_6X_6 (X≡Ge, Sn), (b) CoSn-B35 and (c) $CaCu_5$, showing structural relationships.

TABLE 1. Deviation angle ϕ between the easy direction and the c-axis in RMn_6Sn_6 (R≡Tb–Er)

	ϕ (deg)	
	300 K	2 K
Tb	15	0
Dy	63	45
Ho	90	49
Er	90	90

romagnetic ordering of the Mn sublattice with the Néel temperature T_N varying from 384 to 333 K and from 516 to 473 K for stannides and germanides respectively [3, 6]. As expected, the ordering temperatures of the germanides are higher than those of the stannides, the ordering temperature decreasing with increasing size of the R element. This behaviour probably comes from stronger Mn–Mn coupling owing to shorter Mn–Mn interatomic distances.

A better understanding of the magnetic properties of the RMn_6X_6 compounds is possible by determining the magnetic structures of some diamagnetic R compounds in order to check the magnetic behaviour of the Mn sublattice alone. In addition, it is worth noting that, if the binary compounds MnSn and MnGe do not exist, the RMn_6X_6 compounds (with a diamagnetic R element) can be regarded as a good way to stabilize them and, therefore, to check their magnetic properties comparatively with those of FeSn and FeGe.

In this paper, we report on the magnetic structures of $LuMn_6Sn_6$ and YMn_6Ge_6 derived from neutron diffraction experiments.

2. Sample preparation

Both compounds were prepared from commercially available, high purity elements: Mn (powder, 99.9%), R elements (ingot, 99.9%) and Sn (pieces, 99.99%). Pellets of stoichiometric compositions YMn_6Ge_6 and $LuMn_6Sn_6$ were compacted using a steel die, annealed several times (with grinding and compacting each time) at 1073 K in sealed SiO_2 tubes under argon (0.2 atm) and finally quenched in water. The purity of the final samples was determined by X-ray diffraction, using a Guinier camera (Cu Kα).

Neutron experiments were carried out at the Siloe reactor of the Centre d'Etudes Nucléaires de Grenoble (CENG). Several patterns were recorded in the temperature range 2–300 K with the DN5 multidetector (λ=2.487 Å).

Using the scattering lengths – b_{Ge}=8.185 fm, b_{Mn}=−3.73 fm, b_Y=7.74 fm, b_{Lu}=7.21 fm – and the form factor for Mn given by ref 9, the scaling factor, the $z_{X,Mn}$ atomic positions (X≡Ge, Sn) and the Mn magnetic moment were refined by the MiXeD crystallographic executive for diffraction (MXD) least-square-fit procedure [10]. The MXD program allows

one to fit simultaneously the intensities of the nuclear and magnetic reflections.

3. Neutron diffraction

3.1. YMn_6Ge_6

Several spectra have been collected in the temperature range 2–300 K (Fig. 2). In all the patterns, several superlattice lines are observed (owing to an antiferromagnetic ordering, in agreement with the magnetic measurements) and the remaining lines are characteristic of purely nuclear scattering with no magnetic contributions. The nuclear lines fit well with the $HfFe_6Ge_6$-type structure ($R_{Nucl}=2.4\%$, $Z_{Mn}=0.252$, $Z_{Ge}=0.1607$). The weakness of the ($hk1$) lines relative to the ($hk3$) lines accounts well for the close values of the Ge and Y Fermi (scattering) lengths and to the atomic positions $z_{Ge}=\approx 1/6$, 1/2, 0; $z_{Mn}=\approx 1/4$ and $z_Y=1/2$ (Table 2), which lead to the following structure factors: $F_{hk1}\approx K(b_{Ge}-b_Y)$ and $F_{hk3}\approx K(2b_{Ge}+b_Y)$.

At 300 K, the Bragg angles of the superlattice lines can all be indexed on the basis of a magnetic unit cell twice as large as the crystal unit cell by doubling the c axis (*i.e.* a wave vector $\boldsymbol{k}=(0.\ 0,\ 1/2)$). The absence of (0, 0, $l/2$) magnetic lines suggests that the moments are parallel to the c axis. Considering both Mn layers (lying in $z\approx 1/4$ and $z\approx 3/4$; Figs. 1 and 3(b)), two magnetic arrangements along the c-axis are possible:

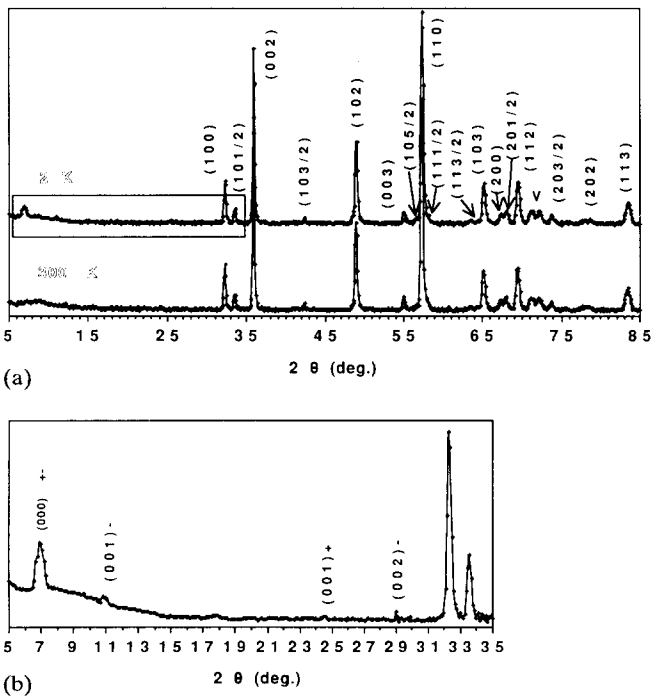

Fig. 2. (a) Neutron diffraction patterns of YMn_6Ge_6 at 300 and 2 K. (b) Detailed view of the neutron diffraction pattern of YMn_6Ge_6 at 2 K, showing the occurrence of four extra lines attributed to the incommensurate basal plane component.

TABLE 2. RMn_6X_6 ($HfFe_6Ge_6$-type structure, *P6/mmm*) data for atomic positions [2]

Atom	Position	Symmetry	x	y	z
R	1(b)	6/*mmm*	0	0	1/2
Mn	6(i)	*mm*	1/2	0	≈0.25
X_1	2(e)	6*mm*	0	0	≈0.16
X_2	2(d)	62*m*	1/3	2/3	1/2
X_3	2(c)	62*m*	1/3	2/3	0

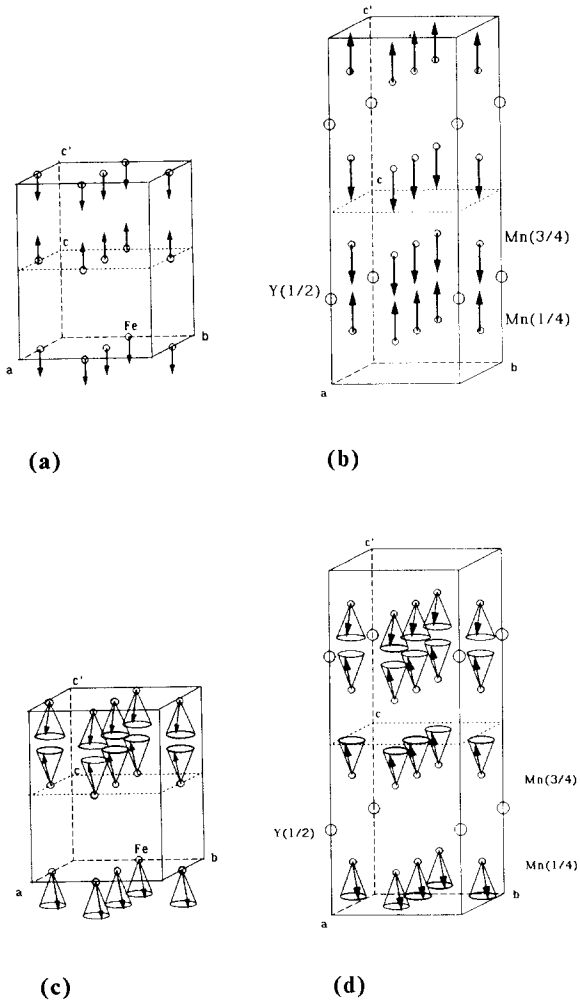

Fig. 3. Magnetic structures of (a) FeGe (HT) at 300 K, (b) YMn_6Ge_6 (HT) at 300 K, (c) FeGe (BT) at 4 K and (d) YMn_6Ge_6 (BT) at 2 K. c' is for the magnetic unit cell.

Mn(+)–R–Mn(−)–Mn(−)–R–Mn(+) or Mn(+)–R–Mn(+)–Mn(−)–R–Mn(−). The best refinement leads us to retain the first of these arrangements with an Mn magnetic moment of $\mu_{Mn}=1.82(3)\mu_B$.

At this point, it should be noted that the choice between the two different magnetic arrangements strongly depends on the shift of the z_{Mn} atomic position from the special position value; *i.e.* 1/4, (in the chemical cell) and on the relative intensities of the magnetic

lines. The refinement of the Mn position, on the basis of the nuclear lines, yields $z_{Mn}=0.252$ at 300 K. The weak shift from the special position implies that the choice between the two models is relatively ambiguous (the $+--+$ array leads to $r_{Mag}=13.4\%$, while the $++--$ arrangement gives $r_{Mag}=18.6\%$) because of the limited accuracy of the present measurement.

Below $T_t=80$ K, four new superlattice magnetic lines appear in the diffraction pattern, while the high temperature $(h, k, l/2)$ lines remain nearly constant (Fig. 2). It is worth noting that no transition is detected in the thermal variation of the susceptibility between T_N and 4 K. The Bragg angles of the new magnetic lines are consistent with an incommensurate magnetic ordering and may be indexed as satellites of the nuclear peaks by considering the propagating vector $\boldsymbol{k}'=(0, 0, \tau)$ with $\tau=0.385(1)$. The occurrence of $(00l)^{\pm}$ lines clearly indicates that the moments deviate from the [001] direction. This result suggests that the magnetic structure changes from a collinear c-axis antiferromagnetic structure to a c-axis cone structure with a modulated basal plane component (Fig. 3(d)). It follows that, for the double-cone antiferromagnetic structure that has developed, the intensities of the $(hkl)^{\pm}$ satellites give a direct measure of $\mu_{\perp}$ and the intensities of the $(hkl/2)$ peaks give a measure of $\mu_{\parallel}$. The refinements lead to $0.37(3)\mu_B$ and $1.94(3)\mu_B$ for $\mu_{\perp}$ and $\mu_{\parallel}$, respectively, yielding a cone semi-angle (α) of about 11°. Furthermore, the phase angle difference between two adjacent Mn layers ($z\approx 1/4$ and $z\approx 3/4$ in the chemical cell, Fig. 3(d)) is refined to $\theta=56(15)°$. Therefore, the modulation vector of 0.385(1) (in units of the τ_{001} reciprocal lattice vector (RLV)) corresponds to a spiral-turn angle (ϕ) of about 125° between adjacent

TABLE 3. Calculated and observed intensities, lattice parameters and different adjustable parameters for YMn_6Ge_6 at 300 and 2 K

$h\ k\ l$	2 K		300 K	
	I_c	I_o	I_c	I_o
$0\ 0\ 0^+$	2.43	2.44(9)	–	–
$0\ 0\ 1^-$	0.67	0.66(15)	–	–
$0\ 0\ 1^+$	0.63	0.64(29)	–	–
$0\ 0\ 2^-$	1.87	1.7(4)	–	–
0 0 1	0.22	–	0.27	–
1 0 0				
$1\ 0\ 0^+$	119.4	112(2)	118.8	120(2)
1 0 1/2	39.5	38(2)	35.6	35(2)
0 0 2	531.7	538(3)	532.2	551(6)
1 0 1	0.84	–	0.77	–
1 0 3/2	22.4	20(2)	20.7	22(3)
1 0 2	550.2	563(5)	549.3	565(6)
0 0 3	102.2	88.3	105.5	106(3)
1 0 5/2	9.0	–	7.8	–
1 1 0	2109.2	2068(11)	2109.9	2072(10)
1 1 1/2	25.6	35(5)	23.0	32(5)
1 1 3/2	19.2	21(4)	17.7	26(6)
1 0 3	578.4	583(7)	572.0	568(6)
2 0 0	108.6	141(5)	108.7	131(6)
2 0 1/2	187.9	197(5)	169.3	162(5)
1 1 2	681.9	699(7)	683.2	696(7)
1 0 7/2	4.0	–	3.8	–
2 0 3/2	146.6	142(6)	135.5	145(6)
1 1 5/2	10.5	–	9.4	–
0 0 4	10.5	–	10.6	–
2 0 2	44.3	59(15)	44.6	56(16)
1 1 3	573.9	599(19)	567.8	591(17)
R (%)	4		3.7	
a (Å)	5.194(2)		5.209(3)	
c (Å)	8.095(4)		8.111(5)	
$\boldsymbol{k}$	(0, 0, 0.384)		–	
z_{Ge}	0.1607(8)		0.1607(8)	
z_{Mn}	0.2512(12)		0.2521(11)	
μ_{Mn} (μ_B)	1.95(4)		1.82(3)	
θ (deg)	11(1)		–	
α (deg)	56(13)		–	

Mn–(R–X)–Mn layers and of about 14° between Mn–(X)–Mn layers (Figs. 1 and 3(d)), corresponding to a repeat distance of about 105 Å.

Table 3 gives the observed and calculated intensities, together with the lattice constants and the different adjustable parameters.

3.2. $LuMn_6Sn_6$

Several spectra have been collected in the temperature range 2–300 K (Fig. 4). At 300 K, the superlattice lines observed (owing to an antiferromagnetic ordering, in agreement with the magnetic measurements) can all be indexed on the basis of a magnetic unit cell (m) twice as large as the chemical cell (c) by doubling the c axis, while the remaining lines are characteristic of purely nuclear scattering with no magnetic contributions. The nuclear lines fit well with the $HfFe_6Ge_6$-type structure ($R_{Nucl}=4.2\%$, $z_{Mn}=0.256$, $z_{Sn}=0.1664$).

The occurrence of (00l) lines clearly indicates that the Mn moments deviate from the c-axis direction. Moreover, in the magnetic cell, the Mn atoms related by the lattice translation along c ($z^m_{Mn}=(z^c_{Mn}/2)$ and $1/2+z^m_{Mn}$) have to be strictly antiferromagnetically coupled, whereas the angle α between the moments of the Mn atoms lying in adjacent layers (z^m_{Mn} and $1/2-z^m_{Mn}$) is a refinable parameter. The best refinements clearly show that the Mn magnetic moments lie in the (001) plane. Within the standard deviations, the refined value of α (172(28)°) yields a collinear antiferromagnetic structure with the Mn(+)–R–Mn(−)–Mn(−)–R–Mn(+) arrangement along the c axis, as shown in Fig. 5(b). The calculated value of the Mn magnetic moment ($\mu_{Mn}=1.33(1)\mu_B$) is slightly smaller that that observed in YMn_6Ge_6 ($1.82(3)\mu_B$), which is in agreement with the Néel temperatures observed in these two compounds ($T_N=353$ K for $LuMn_6Sn_6$ compared with $T_N=480$ K for YMn_6Ge_6) for room temperature measurements. Table 4 gives the observed and calculated intensities, together with the lattice constants and the different adjustable parameters.

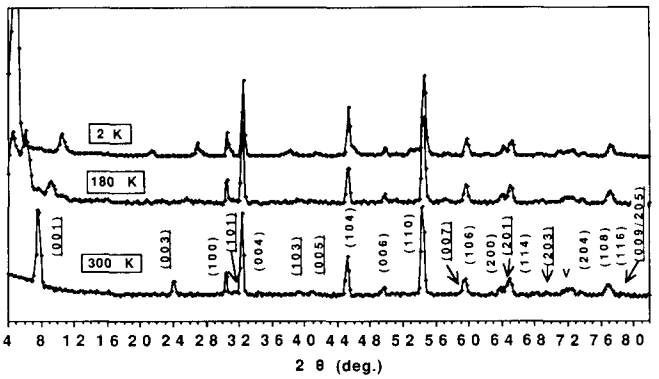

Fig. 4. Neutron diffraction patterns of $LuMn_6Sn_6$ at 300, 180 and 2 K.

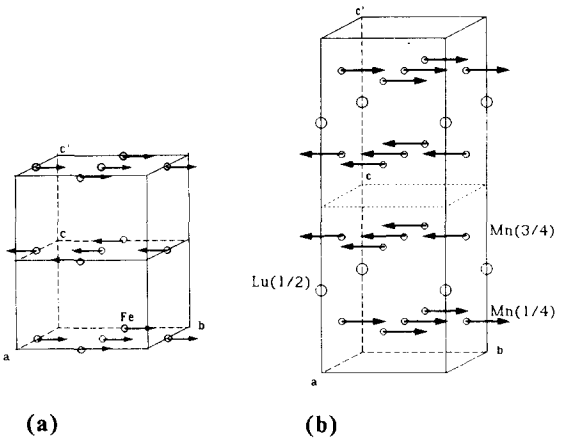

Fig. 5. Magnetic structures of (a) FeSn (HT) at 300 K and (b) $LuMn_6Sn_6$ (HT) at 300 K. c' is for the magnetic unit cell.

TABLE 4. Calculated and observed intensities, lattice parameters and different adjustable parameters in $LuMn_6Sn_6$ at 300 K

h k l	I_c	I_o
0 0 1	48.9	48(1)
0 0 2	0.0	2.1(1)
0 0 3	51.1	55(1)
1 0 0	146.3	148(2)
1 0 1	14.7	20(5)
0 0 4	522.5	525(4)
1 0 2	2.4	–
1 0 3	19.2	23(3)
0 0 5	29.1	32(4)
1 0 4	470.4	481(6)
1 0 5	12.7	13(7)
0 0 6	111.7	104(5)
1 1 0	1809.3	1784(12)
1 1 1	8.9	–
1 1 2	2.4	–
0 0 7	31.5	37(8)
1 0 6	473.4	449(9)
1 1 3	10.4	14(8)
2 0 0	151.2	200(11)
1 1 4		
2 0 1	522.9	546(13)
1 0 7	15.5	9(10)
2 0 2	−2.1	–
0 0 8	−4.6	–
2 0 3	75.6	64(14)
1 1 5	7.2	–
2 0 4	160.2	172(15)
1 0 8		
1 1 6	492.2	532(19)
0 0 9		
2 0 5	60.5	85(20)

$R=3.9\%$; $z_{Sn}=0.0832(8)$; $z_{Mn}=0.128(1)$; $a=5.507(2)$ Å; $c=8.994(5)$ Å; $\mu_{Mn}=1.33(1)\mu_B$; $\theta=8(28)°$.

Below 200 K, neutron diffraction patterns (Fig. 4) are characterized by the vanishing of the high temperature magnetic lines and the occurrence of new magnetic contributions. These new peaks could be

indexed as satellites of the nuclear lines, with at least two wavevectors $k_i = (0, 0, \tau_i)$. Furthermore, the Bragg angles of these peaks change with the temperature, indicating a thermal variation of k_i. Nevertheless, our preliminary results show that a complex, basal plane, flat spiral probably occurs below 200 K. It is worth noting that such complex magnetic behaviour is also encountered over the whole ordered temperature range for the two other diamagnetic rare earth stannides, *i.e.* for $ScMn_6Sn_6$ and YMn_6Sn_6 [11]. Attempts to establish the low magnetic structure of $LuMn_6Sn_6$ are in progress.

4. Discussion and conclusions

The determination of the magnetic structure of YMn_6Ge_6 and $LuMn_6Sn_6$ (*i.e.* diamagnetic elements) provides useful information about the magnetic behaviour of the Mn sublattice in the $HfFe_6Ge_6$-type structure RMn_6X_6 compounds. According to the present neutron diffraction study, the magnetic structures of YMn_6Ge_6 and of $LuMn_6Sn_6$ at room temperature are characterized by a stacking of ferromagnetic (001) Mn planes, antiferromagnetically coupled along the c axis in magnetic unit cells twice the size of the chemical cells, with the same coupling sequence Mn(+)–R–Mn(−)–Mn(−)–R–Mn(+). The direct Mn–Mn interactions are ferromagnetic, while the superexchange Mn–(R–X)–Mn and Mn–(X)–Mn interactions (Figs. 3 and 5) are antiferromagnetic and ferromagnetic respectively. Furthermore, $LuMn_6Sn_6$ exhibits an easy plane, at least at high temperatures (above 200 K), while an easy c axis prevails throughout the temperature range from room temperature to about 2 K in YMn_6Ge_6. In this case of YMn_6Ge_6, the moment rotation between successive layers of Mn corresponds to an exchange energy apparently sufficient to sustain long-range order with a periodicity of about 105 Å and certainly indicates that the basal plane magnetic anisotropy must be very small.

Moreover, the magnetic anisotropy observed in these compounds can be considered to be the behaviour resulting from the Mn sublattices, since Y and Lu are non-magnetic. The substituent effect (Ge ↔ Sn) shows that Ge makes a negative contribution to the magnetic anisotropy, while Sn makes a positive contribution. Similar effects are observed by T–T substitution in R_2T_{17} and RT_5 compounds. It should also be noticed that the + − − + configuration found in the $LuMn_6Sn_6$ compound also occurs in YMn_6Ge_6 with a lower accuracy (see above). In the YMn_6Ge_6 compound, within the standard deviations, the ferromagnetic coupling through the 'X plane' remains for the incommensurate basal plane component, as observed in the stannide, since the refined spiral-turn angles yield spin rotations of 125(15)° from Mn(1/4) to Mn(3/4) through the 'R–X plane' and 13(15)° from Mn(3/4) to Mn(5/4) through the 'X plane'.

In another way, these results allow comparisons between the CoSn-type-structure Fe germanide and stannide and the corresponding $HfFe_6Ge_6$-type-structure rare earth Mn germanides and stannides, as well as a better understanding of the macroscopic properties of RMn_6Ge_6 compounds.

In the introduction, we have emphasized the straight structural relationships between the hexagonal binary FeSn and FeGe and the RMn_6X_6 (R ≡ Y, Lu; X ≡ Ge, Sn) compounds. The magnetic structures of FeSn and FeGe are illustrated in Figs. 3 and 5 [12–17]. It clearly appears that there are strong similarities between the binary and ternary germanides, on the one hand, and the corresponding stannides, on the other hand, with the same change of the easy magnetization direction from the c axis to the (001) plane by substituting Sn for Ge.

These correlations are still enhanced by the low temperature behaviour of the germanides, characterized by the formation of double cone-structures below 55 K and 80 K in FeGe-B35 [15, 17] and YMn_6Ge_6 respectively. It seems that the inserted R element acts as an electron donor, yielding the same electronic features in both classes of compounds FeX and RMn_6X_6 (X ≡ Ge, Sn).

The occurrence of modulated magnetic ordering with long periodicity is a common characteristic of numerous intermetallic compounds, such as MnSi, $Fe_{1-x}Co_xSi$, FeGe-B20, FeGe-B35 and FeGe monoclinic [18–20]. The long-period helical magnetic structures in MnSi and FeGe-B20 have been shown to be consequences of ferromagnetic Dzyaloshinsky instability [21]. Such instability may occur only in certain crystal structures which lack inversion symmetry. Since YMn_6Ge_6 is centrosymmetric, it may be interesting to consider a lowering of symmetry below 80 K in this compound. (A symmetry analysis of the antiferromagnetic phase transitions in hexagonal FeGe-B35 can also be found in ref. 22.) However, it should be noted that a spin–flip effect occurs in FeSn below 70 K [13, 14], while complex, flat spiral structures occur below 200 K in $LuMn_6Sn_6$ and over the whole range of temperatures in $ScMn_6Sn_6$ and YMn_6Sn_6.

Previously, we have largely described and discussed the magnetic couplings and easy axis directions found in the RMn_6Sn_6 compounds [7, 8, 23], (see also Section 1). The magnetic structure of $LuMn_6Sn_6$ (easy plane, Mn sublattice), determined in this paper, clearly confirms our conclusions and, particularly, that the magnetocrystalline anisotropy of these RMn_6Sn_6 compounds arises from a combination of the contributions from the transition metal sublattice and the rare earth sub-

lattice. The Tb sublattice anisotropy is apparently dominant, even at room temperature, while the partial reorientation of the Mn sublattice for Dy and Ho is evidence of the strong anisotropy of the easy magnetization axis of Dy(Ho) and Mn, from which the observed behaviour probably originates (Table 2). No conclusion can be drawn for the Er compound, since an easy plane usually prevails with this element. However, we must take into account the recent work of Dirken *et al.* [24], relating to the effect of the second-order crystal-field parameter A_2°. The low value obtained by these authors in $GdMn_6Sn_6$ suggests that the anisotropic behaviour of the RMn_6Sn_6 compounds will be determined only to a limited extent by the second-order parameter, leaving an important role for the parameters of higher order than A_2°.

The last remark concerns the anisotropy direction, which probably has a dominant role in the macroscopic magnetic behaviours of the RMn_6X_6 ($X \equiv Ge, Sn$) compounds. Indeed, an easy plane enhances the coupling possibility and favours the exchange interactions. This leads to the helimagnetic structures encountered in the RMn_6Sn_6 compounds ($R \equiv Y$, Sc, Lu at low temperature). Such a magnetic arrangement yields a non-zero molecular field on the rare earth sublattice, giving rise to the polarization of the rare earth moment, with the resulting ferrimagnetic structures observed for $TbMn_6Sn_6$, $HoMn_6Sn_6$, $DyMn_6Sn_6$ and $ErMn_6Sn_6$ below 50 K. However, in the germanides, the Mn moments, frozen along the c axis by uniaxial anisotropy with an Mn(+)–R–Mn(−)Mn(−)–R–Mn(+) coupling sequence, yields a collinear antiferromagnetic structure with zero molecular field on the rare earth sublattice. From this point of view, the knowledge of the magnetic structures of some RMn_6Ge_6 compounds will be of great interest. Neutron diffraction studies of $NdMn_6Ge_6$ and $TbMn_6Ge_6$ are in progress.

References

1 B. Malaman, G. Venturini and B. Roques, *Mater. Res. Bull., 23* (1988) 1629.
2 B. Chafik El Idrissi, G. Venturini and B. Malaman, *Mater. Res. Bull., 94* (1991) 35.
3 G. Venturini, R. Welter and B. Malaman, *J. Alloys Comp., 26* (1991) 431.
4 R. R. Olenitch, L.G. Akselrud and Ya.P. Yarmoliuk, *Dopov. Akad. Nauk Ukr. RSR, Ser. A, 2* (1980) 84.
5 P. Villars and L.D. Calvert, *Pearson's Handbook of Crystallographic Data for Intermetallic Phases,* American Society for Metals, Materials Park, OH, 1991, 2nd edn.
6 G. Venturini, B. Chafik El Idrissi and B. Malaman, *J. Magn. Magn. Mater., 94* (1991) 35.
7 G. Venturini, B. Chafik El Idrissi, B. Malaman and D. Fruchart, *J. Less Common Met., 175* (1991) 143.
8 B. Chafik El Idrissi, *Thesis,* Université de Nancy, France, 1993.
9 C.G. Shull and Y. Yamada, *J. Phys. Soc. Jpn., 22* (1962) 1210.
10 P. Wolfers, *J. Appl. Crystallogr., 23* (1990) 554.
11 B. Chafik El Idrissi, personal communication.
12 K. Yamaguchi and H. Watanabe, *J. Phys. Soc. Jpn., 22* (5) (1967) 1212.
13 S. Ligenza, *Phys. Status Solidi B, 45* (1971) 721, 775.
14 L. Häggström, T. Ericsson, R. Wäppling and K. Chandra, *Phys. Scr., 11* (1975) 47.
15 H. Watanabe and N. Kunitomi, *J. Phys. Soc. Jpn., 21* (1966) 1932.
16 J.B. Forsyth, C. Willkinson and P. Gardner, *J. Phys. F, 8* (1978) 2195.
17 J. Bernhard, B. Lebech and O. Beckman, *J. Phys. F, 14* (1984) 2379.
18 C. Willkinson, F. Sinclair and J.B. Forsyth, *Proc. 5th Int. Conf. on Solid Components of Transition Elements,* Extended abstracts, Upsalla, 1976, p. 158.
19 D. Fruchart, B. Malaman, G. Le Caër and B. Roques, *Phys. Status Solidi A, 78* (1983) 555.
20 G.P. Felcher, J.D. Jorgensen and R. Wäppling, *J. Phys. C, 16* (1983) 2195.
21 P. Bak and M. Hogh Jensen, *J. Phys. C, 13* (1980) L881.
22 B. Lebech, Yu. A. Izyumov and V. Syromiatnikov, *J. Phys. C, 20* (1987) 1713.
23 G. Venturini, R. Welter and B. Malaman, *J. Alloys Comp., 197* (1993) 101.
24 M.W. Dirken, R.C. Thiel, J.H.V.J. Brabers, F.R. de Boer and K.H.J. Bushcow, *J. Alloys Comp., 177* (1991) L11.